Volcanic disturbance during the recovery of biota in the aftermath of Permian-Triassic boundary mass extinction

Lijian Shen[1,2,3], Yanjun Zhao[1], Zhengjie Zhu[4,5], Chenglin Liu[1], Jian-xin Zhao[2], Yuexing Feng[2], Wei Zhou[2,3], Kim A. Baublys[3], Suzanne D. Golding[3]

1 MNR Key Laboratory of Metallogeny and Mineral Assessment, Institute of Mineral Resources, Chinese Academy of Geological Sciences, Beijing, 100037, China

2 Radiogenic Isotope Facility, School of Earth and Environmental Sciences, University of Queensland 4072, Australia

3 Stable Isotope Geochemistry Laboratory, School of Earth and Environmental Sciences, University of Queensland 4072, Australia

4 Agriculture and Food Engineering College, Baise University, Baise, 533000, China

5 Chongqing Key Laboratory of Exogenic Mineralizaton and Mine Environment, Chongqing Institute of Geology and Mineral Resources, Chongqing 400042, China

Corresponding author: Lijian Shen (shenlijian1019@126.com)

Key Points:

- This study reports high-resolution curves of Sr, S and Th/U ratios of the Early to Middle Triassic marine sediments from the Sichuan Basin
- The geochemical results suggest volcanic eruption imposed severe environmental stress in the aftermath of the End-Permian mass extinction

Abstract

Evaporites and carbonates intercalated with volcanic beds are distributed in the Jialingjiang and Leikoupo Formations straddling the boundary of the Lower and Middle Triassic in the Sichuan Basin. High-resolution curves of $^{87}Sr/^{86}Sr$ ratios and $\delta^{34}S_{sulphate}$ of marine sediments show the study section has relatively stable isotopic compositions of S and Sr except for the volcanic bed. The abrupt positive shift of $^{87}Sr/^{86}Sr$ ratios and negative shift of $\delta^{34}S_{sulphate}$ occurred in the volcanic layer. The Sr isotopic curve defines a rough age range of 244 to 248 Ma. The volcanic bed is characterized by high anhydrite Th/U ratios, indicating a strong anoxic environment. The volcanic eruptions released a huge amount of CO_2 and SO_2, which could lower temperature first by sulphate aerosols and induce subsequent climate warming by greenhouse gases. This cooling-warming cycle has triggered the overturn of the deep anoxia seawater. The synergistic effects of degassing of gases (CO_2 and SO_2) and overturn of the deep anoxia seawater have caused the negative shifts of $\delta^{34}S_{sulphate}$, and anoxic event during the volcanic eruption. Meanwhile, volcanic eruptions and associated acid rain could have enhanced the continental weathering, resulting in an increasing flux of radiogenic ^{87}Sr. Furthermore, volcanic eruptions and related environmental changes could have imposed severe stress on the full recovery of the ecosystem since the End-Permian mass extinction, which is corroborated by fossil records.

1 Introduction

The End-Permian mass extinction (EPME) occurred at some 252.3 million years ago (Shen et al., 2011), during which 80-96% of marine animal species and 70% of terrestrial vertebrate species went extinct (Chen & Benton, 2012). The EPME was the largest biotic catastrophe among the last 549 million years, and biotic diversity did not recover to pre-extinction levels until the Middle Triassic (Payne et al., 2004; Shen et al., 2011). After the EPME, high-temperature environment prevailed during the early Triassic, which suppressed the ecosystem recovery (Sun et al., 2012). The ecosystems were rebuilt stepwisely through Early to Middle Triassic (Chen & Benton, 2012) during which temperature dropped significantly (Sun et al., 2012). The establishment of the top-level predator-dominated trophic structure in the Luoping ecosystem in China suggested complete biotic recovery and restoration of marine ecosystems during middle-late Anisian (Hu et al., 2011).

The volcanic ash bed, which subsequently transformed into a clay-type, illite-enriched sedimentary rocks (namely the “green bean” rock, Tan et al., 2014), are widely distributed in

South China during the middle to late Triassic period. This layer is defined as the boundary of the Middle and Late Triassic (Zhu, 1990). Major mass extinctions are closely associated with flood volcanism, for instance, Permian-Triassic and late Devonian mass extinctions (Renne & Basu, 1991; Courtillot et al., 1996; Olsen, 1999). During the period of full recovery of the ecosystem until middle-late Anisian, what effects could the volcano activities related to the "green bean" rocks have imposed on the environments are still unclear.

Marine sediments are well-developed during Early to Middle Triassic in the Sichuan basin, South China (Chen & Chu, 1988), consisting mainly of rhythmically alternating carbonates and anhydrites with multiple cycles (Li et al., 2014). The "green bean" rock is intercalated within this section. Those sequences offer an opportunity to investigate the marine environmental changes caused by volcanic activities.

Sulfur is cycled through a variety of environmental and biological reservoirs (Sim et al., 2015), and Sr can serve as a tool for marine sediment correlation (McArthur et al., 2012). In this paper, we present a crucial study on the Early-Middle Triassic boundary using S and Sr isotopic systematics and redox index of high-resolution record of evaporitic sequence in the Sichuan Basin, South China. Published carbonate-associated sulphate (CAS) records often show a large scatter of values and some studies have shown that diagenesis can significantly alter the original signal (Present et al., 2015). Certain analytical methods may lead to erroneous results due to the incomplete elimination of non-CAS sulphur-bearing components (Wotte et al., 2012). Claypool et al. (1980) proposed that evaporite δ34S is generally accepted as recording true seawater-sulphate isotopic values. Thus it is desirable to confirm seawater sulphur isotopes with the analysis of sulphate evaporites. In this study, Sr and S isotopes were analysed by using carbonates/anhydrites and pure anhydrites respectively, to obtain the true seawater Sr and S isotopes. C isotope geochemistry is referenced to interpret the evolution of paleoclimate and marine environments during the transition of the Early to Middle Triassic period as well.

2 Geologic Background

The South China block (Fig. 1A) contains the Sichuan basin in the northwest (Fig. 1B), which was located near the equator in the eastern Paleotethys Ocean during early Triassic (Fig. 1C). Marine sedimentation dominated in the Sichuan Basin from the Upper Sinian to the Middle Triassic. During the earliest Permian, platform carbonates were deposited due to marine transgression with a typical thickness of 300-500 m. The Upper Permian consists of platform

carbonates with alternating marine and terrestrial coal measure (Cai et al., 2003). The Lower and Middle Triassic were subdivided into three formations (Fig. 1D), Feixianguan (T_1f), Jialingjiang (T_1j), and Leiloupo (T_2l), from the base upward, and are predominantly composed of platform carbonates and evaporites. Basin-wide anhydrite beds occur in Jialingjiang and Leikoupo Formations, whereas Feixianguan Formation contains little anhydrite (Cai et al., 2003). The Sichuan Basin was uplifted during the middle to late Triassic as a result of Indo-China movement. The Upper Triassic sediments are composed of freshwater lacustrine-alluvial clastics with local coal beds.

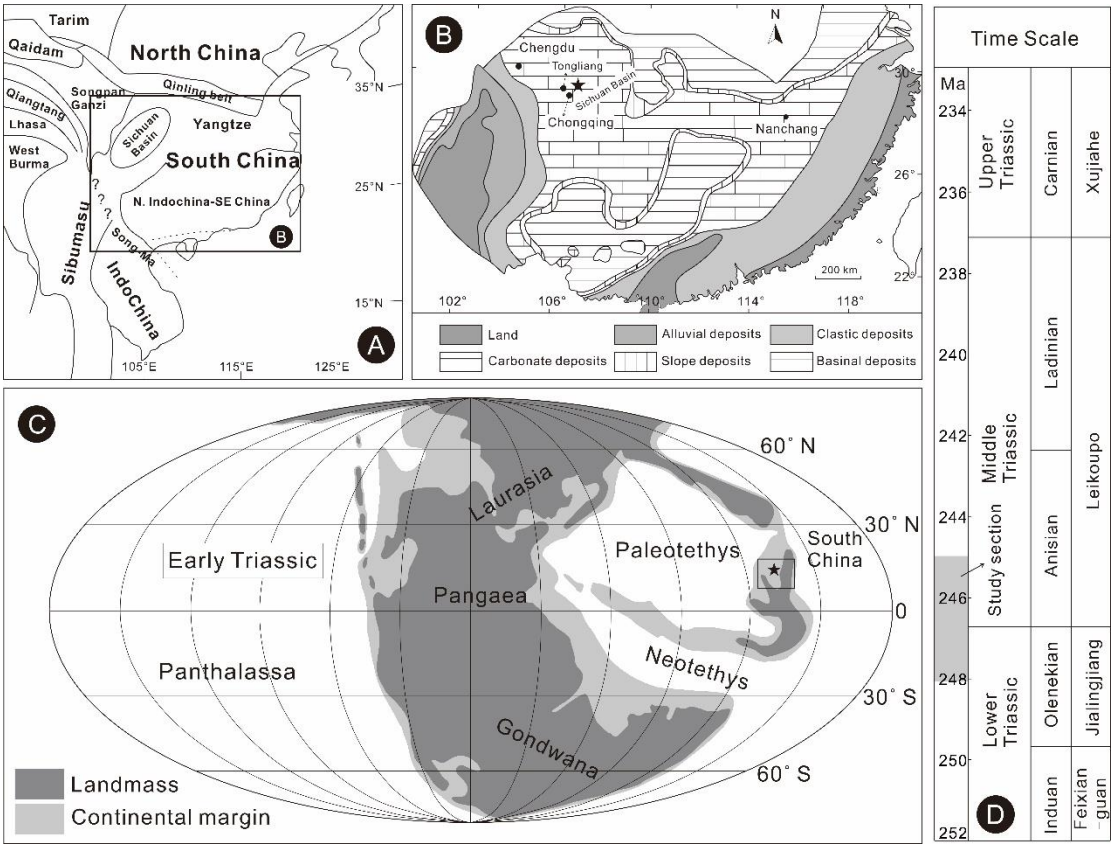

Figure 1. Schematic maps of the study area. A, Principal continental terranes that form present-day Southeast Asia (Modified from Carter et al., 2001). B, Map showing the study site signified by the star (modified from Song et al., 2015). C, Paleogeographic atlas illustrating the position of South China during Early Triassic (modified from Scotese et al., 1997). D, Evaporite section in the Sichuan Basin.

3 Materials and Methods

Seventy-six samples were collected from different gypsum/carbonate layers at approximately 1-3 m intervals, evenly covering a section of 200 m thick from drill core ZK3. The entire section consists mainly of carbonates (Fig. 2A, C), anhydrites (Fig. 2C, D).

Carbonates are mainly composed of calcite and dolomite (Fig. 2B). Carbonates generally have black tonalities, and display massive and layered characteristic, whereas anhydrite layers are white, and have fibrous texture (Fig. 2C). Nodular and massive anhydrites are found within some carbonate layers (Fig. 2D). Some anhydrite layers contain minor amounts of halite. The "green bean" rock layer was developed in the upper part of our study section. This layer could be identified by its distinct features, such as greenish colour (Fig. 2E), quartz-nuclei with approximately 1 to 3 mm in diameter. Thin-layered or lensed carbonates and/or anhydrites were intercalated in the "green bean" rock.

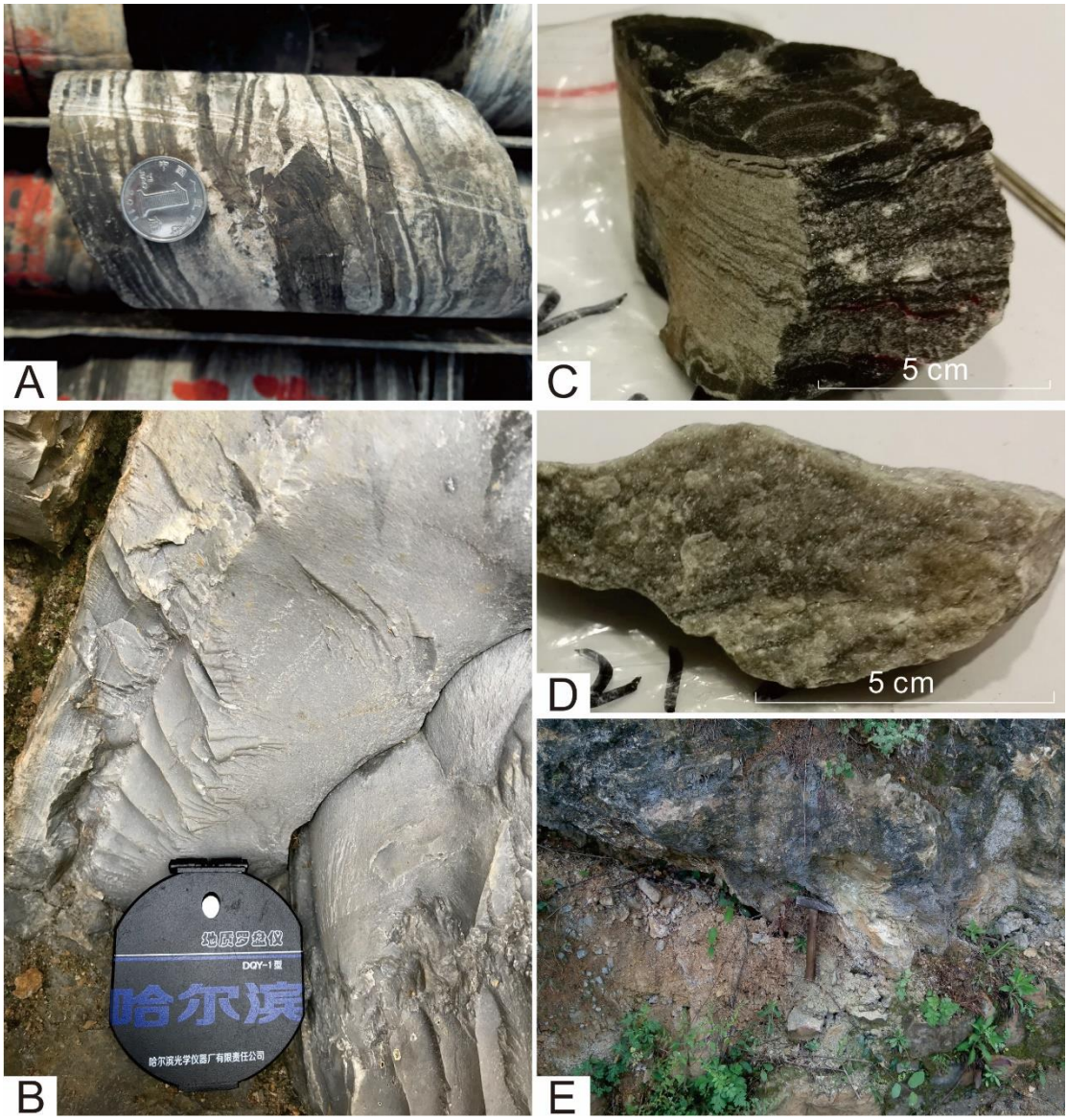

Figure 2. Characteristics of marine sediments and "green bean" rock during the latest Early Triassic to the immediate Middle Triassic in Sichuan Basin. A, carbonates in drill core; B,dolomite in field outcrop; C, alternating

anhydrite and carbonate layers in drill core; D, massive anhydrites; E, the "green bean" rock straddles the Early-Middle Triassic.

Based on the relative contents between carbonate and anhydrite, two chemical processes were adopted to acquire the marine chemical signature, i.e., Milli-Q water and dilute acetic acid dissolution. Samples with the predominant mineral of anhydrite (anhydrite samples) were dissolved Milli-Q water at room temperature. Whereas samples with the predominant mineral of carbonates (carbonate samples) were crushed to sand-size particles, and approximately 100 mg of each was digested by dilute acetic acid (1 N) at room temperature. The purpose of the above chemical processes is to eliminate the disturbance of detrital components. We suggest that the Sr isotope composition of carbonates and anhydrite could represent the marine Sr signature in the light of high Sr contents in carbonates and anhydrite. All sample solutions were split into aliquots by weight for analysis. One small aliquot was diluted and preserved for trace elements analyses, and the other larger aliquot was acidified with 1 N HCl for column chemistry and strontium isotopic measurement. Strontium was separated and purified using a Sr-spec resin. The detailed information about Sr separation is depicted in Babechuk and Kamber (2011). The Sr isotopic ratios were measured on a Nu Plasma multi-collector inductively coupled plasma mass spectrometer (MC-ICP-MS) in the Radiogenic Isotope Facility, University of Queensland. The Sr isotopic ratios were corrected for mass discrimination using $^{86}Sr/^{88}Sr=0.1194$. Replicate analyses of separate loads of SRM987 yielded a mean $^{87}Sr/^{86}Sr=0.710237\pm0.000027$ (2σ).

The S isotopic ratios of anhydrites were measured on a stable isotope ratio mass spectrometer coupled in continuous flow mode with an elemental analyser in Stable Isotope Geochemistry Laboratory, University of Queensland. About 15 mg of each sample consisting of nearly pure anhydrite, was encapsulated within tin foil cup and then combusted at 1020 ℃ using column packing mentioned in Baublys et al., (2004). All samples and standards (international and in-lab) were analysed in duplicate and each set of duplicates were separated by a blank to avoid memory effects. All sulfur isotope compositions are expressed in standard delta notation as per mil (‰) deviation from Vienna Canyon Diablo Troilite (V-CDT) with analytical errors of less than 0.2‰.

The trace element concentrations were determined by a Thermo X-series II ICP-MS. The detailed procedure for ICP-MS trace element analysis is given in Niu and Batiza (1997), except that the weighing data were designated roughly. It is practically impossible to analyse the

contents of trace elements accurately based on the above chemical processes. Because the dissolved part of the samples could not be weighed or measured directly. However, the relative concentrations of trace elements are attainable and cogent.

4 Results

The distribution of $^{87}Sr/^{86}Sr$ ratios, $\delta^{34}S_{sulphate}$ values and Th/U ratios are shown in Table 1, Figure 3 and 4. In ascending stratigraphic order, the $^{87}Sr/^{86}Sr$ ratios decrease from approximately 0.70820 to 0.70816, and then climbed to 0.70824 with a small spike. The data decreased again from 0.70824 to approximately 0.70820 and stabilized before the "green bean" rock layer. The "green bean" rocks were characterized by a sharp increase of $^{87}Sr/^{86}Sr$ ratios from approximately 0.70820 to a maximum ratio of 0.70831. The $^{87}Sr/^{86}Sr$ ratios then dropped drastically to about 0.70822 which are similar to those below the "green bean" layer (Fig. 3).

Before the "green bean" rocks, $\delta^{34}S_{sulphate}$ values are relatively stable, with modest fluctuations, from about 30.2‰ to 32.8‰. The "green bean" rock is characterized by a steep decline, from 31‰ on average to 28.6‰. The $\delta^{34}S_{sulphate}$ data then rise to approximately 32‰ again. The $\delta^{34}S_{sulphate}$ values are absent from 2563.95 m to 2599.49 m depth due to the lack of sulphate minerals in this section. We assume that the curve in this period is a stable and relatively smooth interpolation from the segments immediately preceding (Fig. 4).

The study section yielded Th/U mass ratios ranging from 0.0008 to 6.4097 (Fig. 4). The Th/U ratios are extremely low (0.0008 to 0.7525) below the volcanic bed in the study section, except two outliers with values of 1.2069 and 3.3335, respectively. In the "green bean" rocks, the Th/U ratio shifts abruptly to very high values (2.7766 to 6.4097). The interval overlying the "green bean" rocks is marked by a trend toward low values analogous to sections below the "green bean" rock.

Table 1. $^{87}Sr/^{86}Sr$ ratios, S isotope ratios and Th/U ratios of evaporite sequence straddling early to middle Triassic in South China

Sample ID	Depth (m)	Sample type	$^{87}Sr/^{86}Sr$	$\delta^{34}S_{CDT}$ (‰)	Th/U
ZK3-01	2547.98	anhydrite	0.708216	28.6	0.6088
ZK3-02	2528.69	anhydrite	0.708255	30.1	0.0761
ZK3-03	2531.70	anhydrite	0.708219	31.2	0.0517

ZK3-04	2537.55	anhydrite	0.708213	32.2	0.0500
ZK3-05	2534.30	anhydrite	0.708223	32.3	0.0516
ZK3-06	2543.08	anhydrite	0.708224	30.5	0.0843
ZK3-07	2539.53	anhydrite	0.708246	31.3	0.0361
ZK3-08	2544.54	anhydrite	0.708213	29.5	0.2068
ZK3-09	2546.56	anhydrite	0.708213	29.9	0.1154
ZK3-10	2547.87	anhydrite	0.708215	31.6	0.2497
ZK3-11	2549.74	anhydrite	0.708204	29.4	3.3873
ZK3-12	2550.07	carbonate	0.708270	-	2.7766
ZK3-13	2550.44	carbonate	0.708223	-	6.4097
ZK3-14	2550.84	anhydrite	0.708289	31.0	3.0441
ZK3-15	2551.10	carbonate	0.708224	-	3.9841
ZK3-16	2551.42	anhydrite	0.708293	30.8	5.7092
ZK3-17	2551.60	anhydrite	0.708284	30.2	0.7525
ZK3-18	2551.80	anhydrite	0.708277	29.9	0.4183
ZK3-19	2551.93	anhydrite	0.708307	29.1	0.1978
ZK3-20	2552.15	anhydrite	0.708210	30.5	0.0312
ZK3-21	2552.46	anhydrite	0.708189	29.0	0.3716
ZK3-22	2552.79	anhydrite	0.708206	30.3	0.6554
ZK3-23	2554.00	anhydrite	0.708224	28.6	0.5951
ZK3-24	2554.20	anhydrite	0.708225	30.7	0.5244
ZK3-25	2561.18	anhydrite	0.708200	30.8	0.1033
ZK3-26	2555.70	anhydrite	0.708204	30.2	0.2280
ZK3-27	2568.30	carbonate	0.708176	-	0.3490
ZK3-28	2563.95	anhydrite	0.708224	29.0	0.0089
ZK3-29	2562.57	carbonate	0.708198	-	0.0027
ZK3-30	2571.62	carbonate	0.708190	-	0.2373
ZK3-31	2574.34	carbonate	0.708195	-	0.0013
ZK3-32	2576.60	carbonate	0.708181	-	0.0011

ZK3-33	2579.52	carbonate	0.708190	-	0.0017
ZK3-34	2587.51	carbonate	0.708178	-	0.2026
ZK3-35	2581.90	carbonate	0.708190	-	0.0700
ZK3-36	2595.25	carbonate	0.708239	-	0.0008
ZK3-37	2590.50	carbonate	0.708184	-	0.0036
ZK3-38	2599.49	anhydrite	0.708183	30.2	0.0359
ZK3-39	2597.21	anhydrite	0.708222	33.2	0.5146
ZK3-40	2602.66	anhydrite	0.708157	31.4	0.0180
ZK3-41	2603.76	anhydrite	0.708170	31.8	0.0046
ZK3-42	2609.50	carbonate	0.708229	-	3.3335
ZK3-43	2611.07	anhydrite	0.708167	31.6	0.1096
ZK3-44	2615.88	anhydrite	0.708182	31.0	0.1423
ZK3-45	2613.49	anhydrite	0.708171	31.8	0.0691
ZK3-46	2618.39	anhydrite	0.708167	31.7	0.0106
ZK3-47	2620.12	anhydrite	0.708173	31.6	0.0283
ZK3-48	2623.82	anhydrite	0.708164	32.3	0.6145
ZK3-49	2627.80	anhydrite	0.708163	31.7	0.0166
ZK3-50	2631.41	anhydrite	0.708186	31.9	0.0049
ZK3-51	2635.48	anhydrite	0.708166	32.1	0.3003
ZK3-52	2638.40	anhydrite	0.708172	30.3	0.0317
ZK3-53	2641.06	anhydrite	0.708165	30.5	0.0237
ZK3-54	2645.20	carbonate	0.708171	-	0.0110
ZK3-55	2647.93	anhydrite	0.708170	32.1	0.1828
ZK3-56	2650.25	anhydrite	0.708160	30.8	0.0552
ZK3-57	2656.19	anhydrite	0.708163	31.5	1.2069
ZK3-58	2652.05	anhydrite	0.708189	32.5	0.0110
ZK3-59	2657.58	anhydrite	0.708169	32.2	0.0153
ZK3-60	2560.62	anhydrite	0.708173	32.0	0.0068
ZK3-61	2673.94	anhydrite	0.708165	30.6	0.0037

ZK3-62	2675.99	anhydrite	0.708189	32.8	0.0316
ZK3-63	2664.39	anhydrite	0.708181	31.9	0.1814
ZK3-64	2665.42	anhydrite	0.708175	32.5	0.0365
ZK3-65	2664.75	anhydrite	0.708171	32.1	0.1244
ZK3-66	2670.68	anhydrite	0.708174	31.6	0.0343
ZK3-67	2679.00	anhydrite	0.708178	30.3	0.0286
ZK3-68	2680.70	anhydrite	0.708175	32.1	0.0195
ZK3-69	2683.58	anhydrite	0.708176	32.2	0.0341
ZK3-70	2687.78	anhydrite	0.708175	32.4	0.0502
ZK3-71	2689.21	anhydrite	0.708211	32.3	0.0041
ZK3-72	2691.98	carbonate	0.708179	-	0.4431
ZK3-73	2699.80	anhydrite	0.708166	30.6	0.0021
ZK3-74	2703.00	anhydrite	0.708193	30.2	0.1796
ZK3-75	2705.53	anhydrite	0.708203	32.1	0.1912
ZK3-76	2607.65	anhydrite	0.708167	32.6	0.1019

5 Discussions

5.1 Sr isotopes

The Sr isotopic composition of seawater is homogeneous due to its long-time residence time ($\approx 10^6$ yr) compared to the mixing time ($\approx 10^3$ yr; McArthur et al., 2012). The fact that the $^{87}Sr/^{86}Sr$ ratio of seawater has varied over time gives the ability to date and correlate marine sediments (McArthur et al., 2012). Although the delineation of seawater $^{87}Sr/^{86}Sr$ variation through time has been refined recently, a high-resolution data is still needed for dating and correlation (McArthur et al., 2001), especially for comparatively short stratigraphic sections (Veizer et al., 1997). Because the variations and oscillations of Sr isotope composition of a certain section could be assigned to any analogical stratotype, improved resolution of a certain section leading to high order oscillations superimposed on the lower order trends on a global scale. Thus an unusual large peak or specific lithologies are required for definitive correlation.

182 And it is more beneficial to correlate different sequences on intrabasinal and regional scales
183 (Veizer, et al., 1997).

184 The Sr isotopic reference curve used for correlation in this study is composed of $^{87}Sr/^{86}Sr$
185 ratios of well-preserved and well dated conodont samples from South China spanning from the
186 Late Permian to the early Late Triassic (Song et al., 2015). It is suggested that $^{87}Sr/^{86}Sr$ ratios had
187 undergone the steepest and greatest change during the Late Permian to Early Triassic (McArthur
188 et al., 2001), increased 0.00125 in 3.8 Myr until mid-Spathian (Song et al., 2015), thus
189 favourable for stratigraphic correlation.

190 In South China, the $^{87}Sr/^{86}Sr$ profile has a generally decreasing trend during the transition
191 period between the Early and Middle Triassic (Fig. 3, Song et al., 2015). The maximum $^{87}Sr/^{86}Sr$
192 ratio of South China seawater occurred at approximately 245.3 Ma, corresponding to the
193 maximum $^{87}Sr/^{86}Sr$ ratios at the "green bean" rock in this section (Fig. 3). Besides, The U/Pb
194 zircon age of "green bean" rocks in Tongliang County (which is located adjacent to our sampling
195 site, Fig. 1), is of 245.86±0.98 Ma (Sun et al., 2017). There is only one layer of "green bean"
196 rock in the eastern Sichuan Basin, Chongqing (Zhu & Wang, 1986). Thus, the zircon U-Pb age
197 of "green bean" rocks from Sun et al. (2017), in combination with variation of seawater $^{87}Sr/^{86}Sr$
198 ratios in South China (Song et al., 2015) suggest that the formation age of "green bean" rocks
199 from this study is approximately 245 Ma. This result also suggests that the obvious bump of
200 $^{87}Sr/^{86}Sr$ curve of seawater at approximately 245 Ma was very likely caused by volcanic
201 activities.

202 The trend of $^{87}Sr/^{86}Sr$ ratios in our section mimics the shape of the $^{87}Sr/^{86}Sr$ ratios of South
203 China seawater curve, albeit with slightly reduced values (Fig. 3). The minimum and maximum
204 ages of our sequence are constrained to range approximately from 244-245 Ma to 247-248 Ma,
205 with $^{87}Sr/^{86}Sr$ ratio of 0.70822, corresponding to an age range of 244-245 Ma, and $^{87}Sr/^{86}Sr$ ratio
206 0.70820, corresponding to an age range of 247-248 Ma.

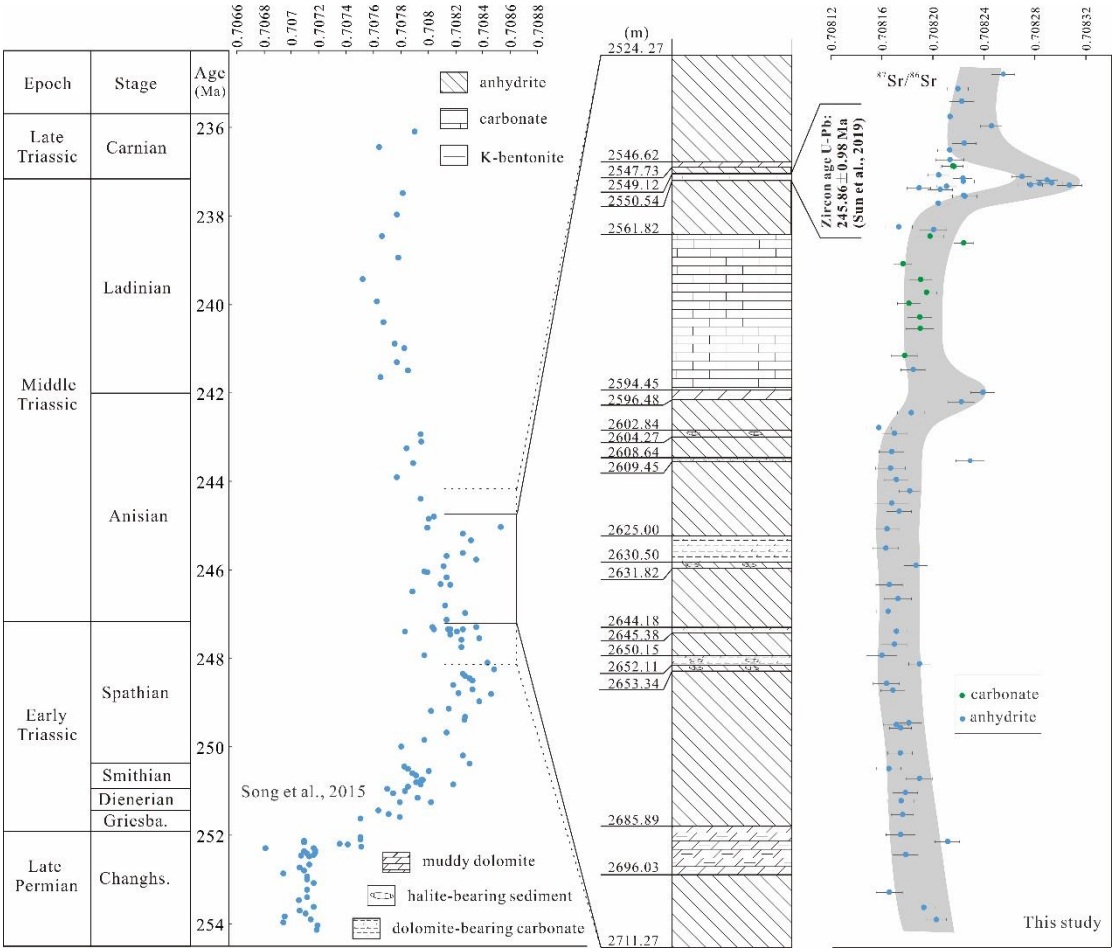

Figure 3. Correlation between Sr isotope compositions of marine sediments in the Sichuan Basin and those of South China seawater (Song et al., 2015).

The Sr isotopic variation of seawater through time is useful for investigating geologic processes such as tectonic uplifts, continental weathering, climate changes, and hydrothermal circulation (McArthur et al., 2001), because there are two major sources for the seawater Sr isotopes: the riverine input caused by continental weathering (high ratios) and volcanic sources (low ratios) (Allègre et al., 2010). The $^{87}Sr/^{86}Sr$ ratios increased continuously from Late Permian to mid-Spathian (Fig. 3), which was likely the result of enhanced continental weathering. One of the major factors controlling continental weathering is orogenic uplifting. The major orogenies around the Sichuan basin consist the accretion of Sibumasu to Indochina-South China (Carter et al., 2001), and the collision of North and South China blocks (Meng & Zhang, 1999), which bound our study area to the Southwest and Northeast, respectively (Fig. 1A). A zircon U-Pb study of the metamorphic basement of Vietnam indicates that a short-lived episode of ductile deformation and high-temperature metamorphism was caused by the accretion of Sibumasu to

Indochina-South China between 258±6 Ma and 243±5 Ma (Carter et al., 2001). However, there is no temporal correlation between the accretion and seawater Sr isotopic changes. The collision ages of North and South China blocks are of middle Paleozoic and Late Triassic (Meng & Zhang, 1999), which could not account for the elevated $^{87}Sr/^{86}Sr$ ratios at the "green bean" rocks. Moreover, the orogeny was only responsible for large scale seawater Sr isotopic changes, not for local changes of Sr isotopic composition of seawater (Richter et al., 1992). Thus, we suggest that the variations of seawater Sr isotopic compositions during the Early to Middle Triassic were not related to orogenic erosions. Alternatively, elevated $^{87}Sr/^{86}Sr$ ratios could have been controlled by enhanced weathering by environmental changes. For instance, a combination of climatic warming, vegetation loss (vegetation provides essential erosion resistance) and intensified hydrological cycle, induced enhanced continental weathering, and increased radiogenic ^{87}Sr flux to the ocean (Song et al., 2015). The Early Triassic has been viewed as an unsuccessful recovery interval after the EPME (Hallam, 1991), and the massive collapse of terrestrial ecosystem could have accounted for the continuous increasing of seawater $^{87}Sr/^{86}Sr$ ratios during most of the Early Triassic.

$^{87}Sr/^{86}Sr$ ratios began to decline following the recovery of vegetation in the middle-late Spathian (Looy et al., 1999). The biotic recovery from Middle Triassic rendered plants to increase on land, which would have reduced continental weathering and its accompanying influx of ^{87}Sr into seawater. During the Middle Triassic, the $^{87}Sr/^{86}Sr$ ratios declined to a stable value (Song et al., 2015), which resembles that of our study section, except for those from volcanic bed (Fig. 3). In the "green bean" rock layer, the $^{87}Sr/^{86}Sr$ ratio culminates in the highest value of 0.708307 and then returns to values slightly higher than the previous values before volcanic bed (Fig. 3). Thus, the maximum $^{87}Sr/^{86}Sr$ ratio at the "green bean" rock indicates strong terrestrial weathering.

By contrast, magmatism has been considered responsible for initiating the marked decrease in seawater $^{87}Sr/^{86}Sr$ ratios (Lo et al., 2002). Therefore, the "green bean" rock and its related volcanic activities could have reduced the seawater $^{87}Sr/^{86}Sr$ ratios, which is not the case in this study. This indicates the continental weathering outbalanced the volcanic activities on Sr isotopic composition. The radiogenic strontium (^{87}Sr) entering the ocean caused by continental weathering have been buffered by ^{87}Sr-depleted components due to volcanic eruptions, indicating the effect of continental weathering was stronger than estimated.

253 **5.2 S isotopes**

254 There are several factors controlling the variation of seawater $\delta^{34}S$ values, namely the
255 precipitation and weathering of evaporites, the output of sulphate via bacterial sulfate reduction
256 (BSR) as sedimentary pyrite and the input of as sulphate derived from the oxidation of sulphides
257 and, the input and output of mantle sulphur along the mid-ocean ridges (Kampschulte & Strauss,
258 2004). The isotope fractionation between evaporitic and seawater sulphate is negligible (Kramm
259 & Wedepohl, 1991). The $\delta^{34}S$ of dissolved component in river is typically thought to be between
260 5 to 15‰ reflecting weathered minerals (Tostevin et al., 2014, and references therein). Magmatic
261 sulphur derived either from mid-ocean ridges or volcanism on land was thought to be
262 quantitatively minor as compared to continental runoff during the Phanerozoic (Gill et al., 2007,
263 and references therein). The continuous BSR under sulphate-limited conditions result in the
264 enrichment in ^{34}S of the remaining dissolved sulphate (Strauss, 1999). Taken together, the factors
265 controlling the variations of S isotopes of seawater include biologic activities, continental
266 weathering and oxidation of sulphides from euxinic facies.

267 The relatively positive $\delta^{34}S_{sulphate}$ values (28.6‰ to 33.2‰) of marine sulphates in this study
268 are consistent with previous research (Chen & Chu, 1988). They demonstrated the remarkably
269 heavy $\delta^{34}S_{sulphate}$ values in the upper Jialingjiang Formation and the lower Leikoupo Formation is
270 a worldwide phenomenon (Chen & Chu, 1988). Claypool et al. (1980) attributed the high $\delta^{34}S$
271 values to extensive BSR in localized stagnant basins. The elevated $\delta^{34}S$ value indicates the Late-
272 Early Triassic ocean was strongly stratified and the deep-water may have been predominantly
273 anoxic. Isotopically light ^{32}S had been sequestered into deep water, resulting in more ^{34}S-
274 enriched shallow seawater. The $\delta^{34}S_{sulphate}$ is high compared with that of western Tethys,
275 indicating a more euxinic influence in the eastern Tethys (Gorjan et al., 2007). On the contrary,
276 the more anoxic condition in the "green bean" rock layer (evidenced by Th/U ratios, discussed
277 below) coincides with a negative shift of $\delta^{34}S$ value, which is contradictory to the BSR
278 mechanism. Therefore, the negative $\delta^{34}S$ value shift at the volcanic bed should have been
279 controlled by other factors.

280 Compared to BSR, enhanced continental weathering, and/or volcanically derived sulphur,
281 and/or oxidation of H_2S due to the overturn of an anoxic ocean could have been responsible for
282 the negative shift (Kaiho et al., 2001). Sr isotope evidence suggests increased continental
283 weathering during the volcanic eruption(s), engendering more ^{34}S-depleted material into the

ocean. By the addition of volcanogenic isotopically light sulfur, enhanced volcanic emissions would have contributed to negative shifts in seawater $\delta^{34}S$ values but with a less or negligible contribution (Adams et al., 2010). In contrast to the estimated supply of volcanogenic sulphur, the reoxidation of H_2S from deeper anoxic portions of the water column would be more than enough to affect a larger shift (Newton et al., 2004).

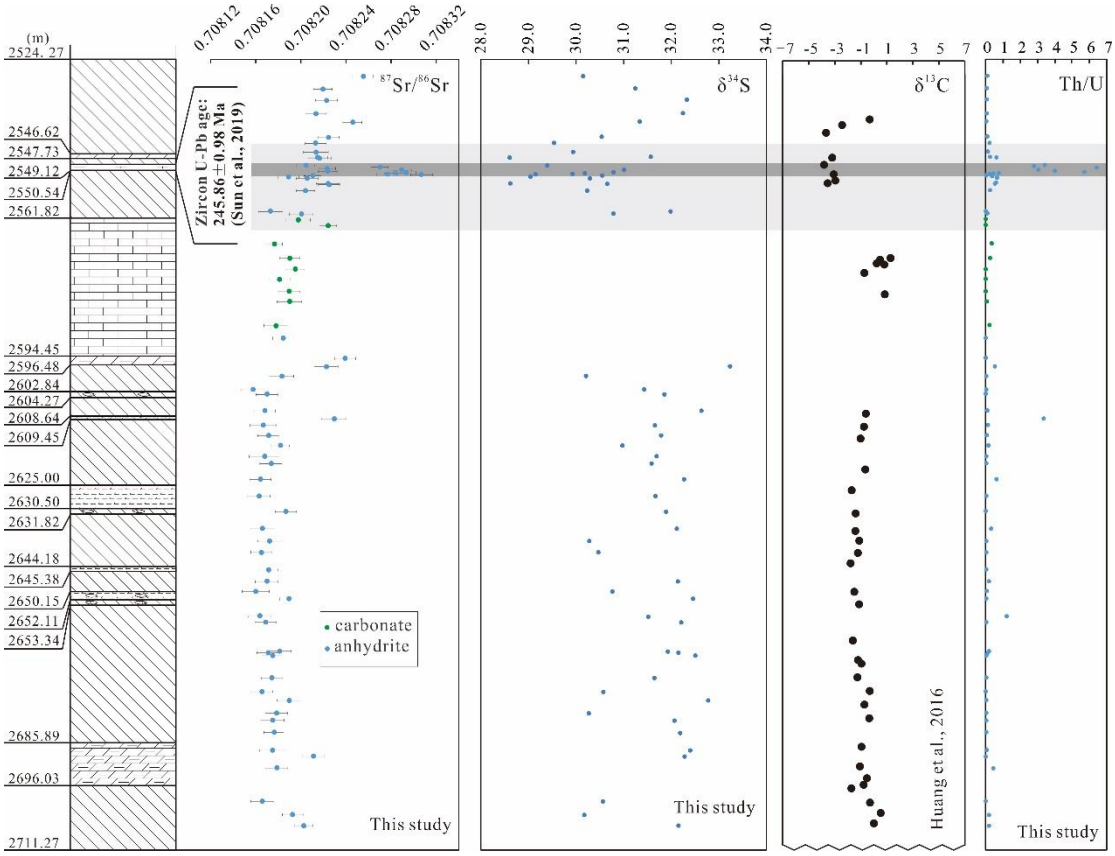

Figure 4. Variations of S, C (Huang et al., 2016) and Th/U ratios of marine anhydrites and carbonates in the Sichaun Basin.

5.3 Implication for environmental changes and disturbance during biotic recovery

According to the variations of S and Sr isotopes, Th/U ratios in this section, 2543.08 to 2563.95 m interval was proposed as the volcano-affected stage (Fig. 4, light grey shadow interval; the dark grey shadow interval indicates the "green bean" rock layer).

As discussed above, continental weathering could have input depleted ^{34}S and relatively high $^{87}Sr/^{86}Sr$ ratio materials into seawater. Thus, there would have been a negative correlation between $\delta^{34}S$ values and $^{87}Sr/^{86}Sr$ ratios if they were controlled predominantly by the weathering process. Fig. 4 shows that $\delta^{34}S$ values and $^{87}Sr/^{86}Sr$ ratios have a visually negative relationship at

the "green bean" rock layer. However, plotting $\delta^{34}S$ versus $^{87}Sr/^{86}Sr$ reveals that there is no negative relationship between $\delta^{34}S$ values and $^{87}Sr/^{86}Sr$ ratios but a slightly positive trend (Fig. 5). This demonstrates that the weathering process was not the underlying or predominant factor controlling the variations of S isotopes.

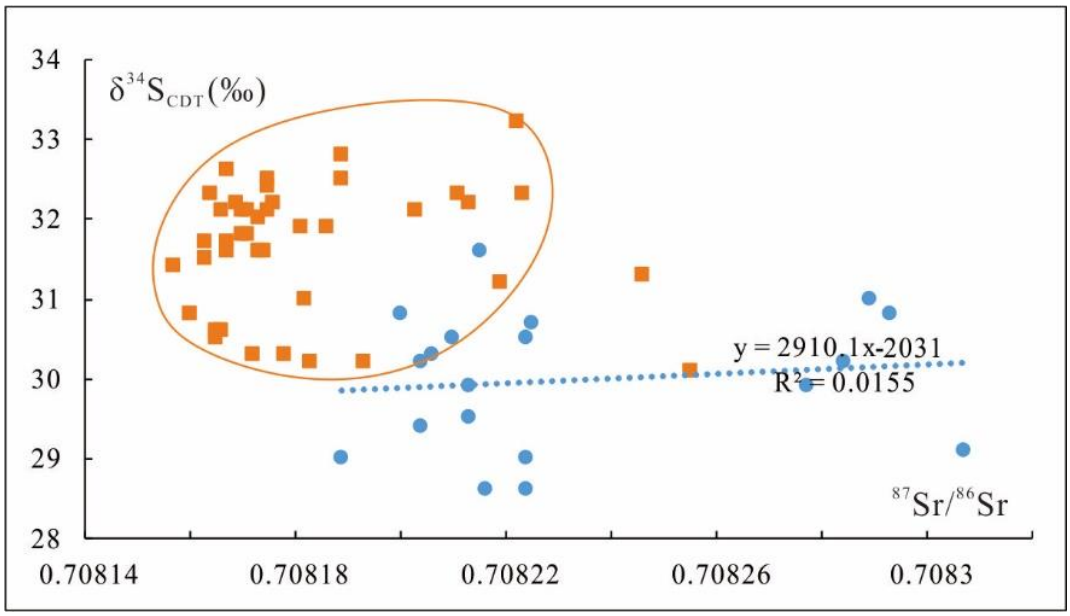

Figure 5. $\delta^{34}S$ values VS. $^{87}Sr/^{86}Sr$ ratios in this study. Blue dots: samples within volcano-affected stage; Orange squares: remainder of the samples.

Th/U ratios can be used to evaluate oceanic redox conditions (Elrick et al., 2017). Th has only one oxidation state (+4), therefore, its concentration in seawater is not affected by water mass redox changes, whereas U is sensitive to redox conditions. In oxidating marine waters, uranium is present mainly as U (+6) in the large uranyl ion (UO_2^{2+}), which forms a part of soluble carbonate and phosphate complexes (Weyer et al., 2008). In reducing environments, reduction to U (+4) leads to the formation of relatively insoluble hydroxide and phosphate complexes and organo-metallic ligands (Klinkhammer & Palmer, 1991). The Th/U ratios of those samples in this study are all derived from relatively dissolved components, i.e., anhydrites and carbonates, instead of insoluble materials. Consequently, an increase in the Th/U ratios of marine carbonates and anhydrites represents enhanced U removal in reducing conditions.

Th/U ratios of samples within the volcano-affected interval are strikingly high compared with those of samples within the remainder of this section. It is suggested that an anoxic environment was prevailed in the volcano-affected section compared with others. Our data argue

for intense anoxia at the volcanic bed and relatively oxygenated condition preceding and following sections of the "green bean" rock layer.

The coupling or/and decoupling of marine carbonates $\delta^{13}C$ and sulphate $\delta^{34}S$ shed light on contemporaneous oceanic and terrestrial processes (Gill et al., 2007). A $\delta^{13}C_{carb}$ excursion was documented previously in this section by Huang et al. (2016). $\delta^{13}C_{carb}$ values of approximately 0‰ at the lower part of this section decreased abruptly at values around -4‰ at the "green bean" rock (Fig. 4). The data then rapidly increased to approximately 0‰ again over the "green bean" rock. This recorded a negative carbon isotope excursion of about -4‰ through the "green bean" rock interval. The negative $\delta^{13}C$ shift in the volcanic bed was not caused by the changes of organic burial or weathering, because both processes are too slow for this extremely rapid event. Brand et al. (2012) proposed that the rapid negative excursion was caused by volcanic discharge of CO_2. Whereas, Payne and Kump (2007) suggested that the introduction of volcanic CO_2 produces small negative carbon isotope excursions. Carbon and sulphur isotope vary sympathetically during this section, reaching their minimum values at the same level, i.e., the "green bean" rock (Fig. 4). Song et al. (2014) proposed that warming events were associated with negative C- and S-isotope shifts and cooling events with positive isotope shifts based on analyses on C and S isotopes of the Early Triassic marine sediments. Seawater temperature may have played an important role on the Early Triassic carbon and sulfur cycles (Song et al., 2014, the mechanism is still not well demonstrated).

The sulphate aerosols formed by oxidation of SO_2 degassing via volcanisms could lower temperature. Then it will be removed from the atmosphere in a short time (1 to 2 years) (Grard et al., 2005). But the degassing of CO_2 could put large amounts of isotopically light carbon into the atmosphere (Eldholm & Thomas, 1993), leading to a globally warm climate (Grard et al., 2005). Meanwhile, the decrease of temperature could induce oceanic overturn and rapid return of HCO_3^-, H_2S and CO_2-charged waters to the surface (Knoll et al., 1996). CO_2 released from the deep ocean combined with that degassing from volcanic eruptions would facilitate a greenhouse climate. A warm climate may have triggered chemocline upward excursions that introduced ^{34}S-depleted sulphide and ^{13}C-depleted dissolved inorganic carbon into the surface water (Kump et al., 2005). Oxidation of H_2S would have generated isotopically light sulphate (Riccardi et al., 2006), leading to a decline of seawater $\delta^{34}S$ values. Moreover, volcanic eruptions ejected isotopically light sulphur into seawater although with limited or negligible effect. These two

processes could have induced the lowering of seawater $\delta^{34}S$ values synergistically (Knoll et al., 1996).

In summary, the negative shifts of carbon and sulfur isotopes at the "green bean" rock interval was very likely caused by the volcano-induced cooling-warming climate cycle. Such a climate cycle could have resulted in an environmental crisis capable of causing mass extinction (Renne et al., 1995).

In the Sichuan Basin, several species of ammonoid and lamellibranchia were present within sequence below the "green bean" rock layer. Ammonoids (including Dinarites sp., D. yunnanensis, Leiophyllites aff. Pitamaha, Hanielites sp., Pseudoceltites sp., Dorieranites sp., Xenoceltites cf. compressus, and Ussuria sp.) and lamellibranchia (including Eumorphotis inaequicostata, Entolium discites mierotis, Pteria cf. murchisoni, Myophoria laevigata, and Anodontophora fassaensis) were present below 15-20 m of the "green bean" rock layer. Only lamellibranchia species were found within sequence above approximately 20 m of the "green bean" rock layer, including Myophoria goldfussia, Eumorphotis (Asoella) illyrica, Eu, subillyrica (Fig. 6, Zhu & Wang, 1986). The number of species of lamellibranchia decreased from 8 to 3, and ammonoids were extinct after the deposition of the "green bean" layer. There were not any species existing in the "green bean" rock layer and its adjacent sequences (Fig. 6).

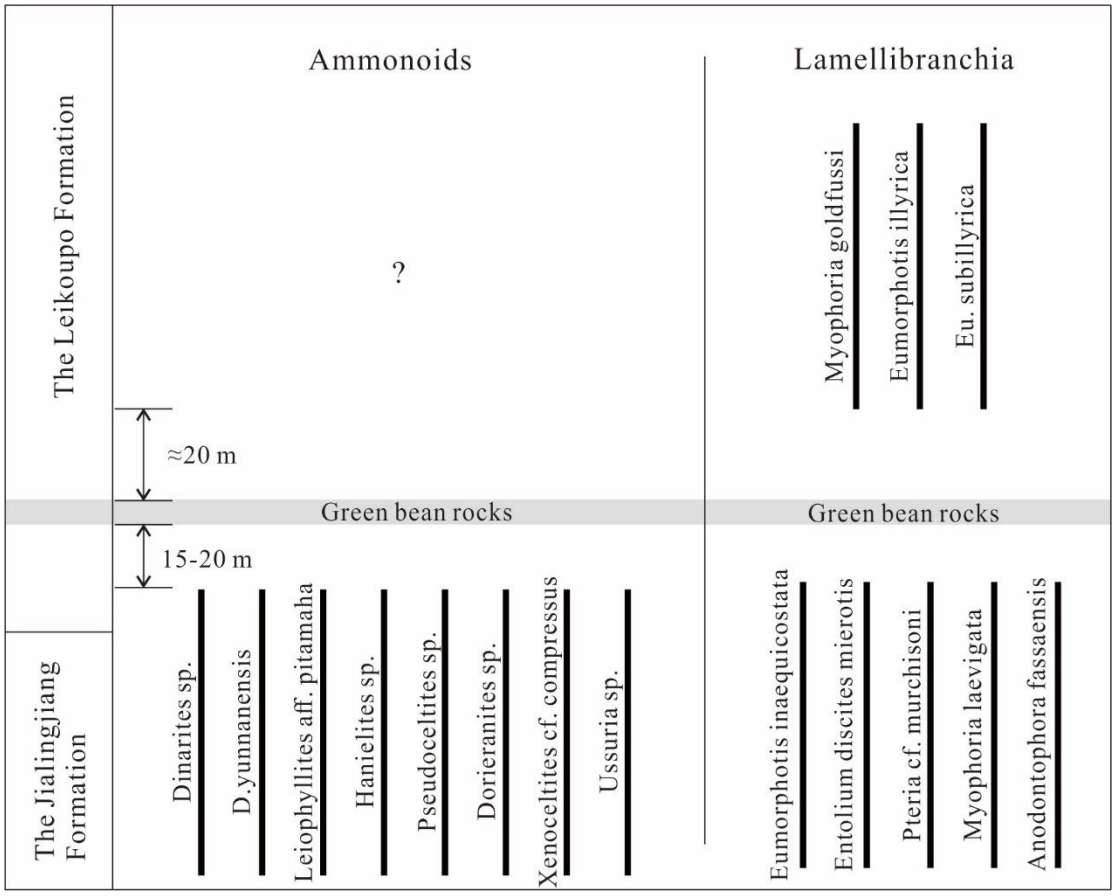

Figure 5. $\delta^{34}S$ values VS. $^{87}Sr/^{86}Sr$ ratios in this study. Blue dots: samples within volcano-affected stage; Orange squares: remainder of the samples.

Obviously, the volcanic activity which formed the "green bean" rocks has imposed severe environmental stress on the marine community in the Sichuan Basin. Some species were killed during the volcano eruption. This scenario is similar to that of Permian-Triassic boundary volcanism which may have played an important role in causing the end Permian mass extinction (Gao et al., 2013). The eruptions of volcanos could have released sufficiently large quantities of CO_2, SO_2, fluorine and chlorine to wreak destruction on atmospheric and biospheric systems (Kamo et al., 2003). Severe atmospheric contamination with H_2SO_4 aerosols produced by gaseous emissions of volcano activities could have resulted in acidic precipitation, causing destabilization of the terrestrial biosphere (Maruoka et al., 2003). When tephra comes in contact with surface waters, acid and metal salts adsorbed onto the tephra surfaces dissolve quickly, releasing acids and metals to the environment (Frogner et al., 2001). Volcano eruptions cause acidification and contamination of soils and surface water, which has a series of impact on vegetation and animals (Kockum et al., 2006). Additional detrimental effect on vegetation may

have derived from large-scale degassing of hydrothermal organohalogens, contributing to stratospheric ozone depletion and increased flux of harmful UV radiation (Visscher et al., 2004).

6 Conclusions

(1) The section composed of alternating marine carbonates and evaporites (mainly anhydrites) with intercalated volcanic bed straddling the boundary of the Lower and Middle Triassic in the Sichuan Basin suggests an age range of approximately 244 to 248 Ma, with volcanic bed of 245.3 Ma.

(2) During the volcanic eruption, enhanced continental weathering and influx of radiogenic ^{87}Sr into seawater increases the $^{87}Sr/^{86}Sr$ ratios of seawater. Degassing of CO_2 and SO_2 and overturn of deep anoxia ocean water induced the negative S and C excursions and anoxic environment in the shallow water.

(3) Volcanic eruption could have caused severe environmental stress on the full recovery of ecosystem and killed some marine species.

Acknowledgments

We thank Faye Lau, Wei Liao, Ai Nguyen for analytical assistance. This study was supported by the 973 Program (2011CB403007), the Chongqing Science and Technology Foundation (Zhu Zhengjie), the National Natural Science Foundation of China (41802111). The data are archived in EarthChem (https://doi.org/10.26022/IEDA/111735).

References

1. Adams, D. D., Hurtgen, M. T., & Sageman, B. B. 2010. Volcanic triggering of a biogeochemical cascade during Oceanic Anoxia Event 2. *Nature Geoscience*, 3(3), 1752-0908. https://doi.org/10.1038/ngeo743
2. Allègre, C. J., Louvat, P., Gaillardet, J., Meynadier, L., Rad, S., & Capmas, F. 2010. The fundamental role of island arc weathering in the oceanic Sr isotope budget. *Earth and Planetary Science Letters*, 292(1), 51-56. https://doi.org/10.1016/j.epsl.2010.01.019

3. Babechuk, M. G., & Kamber, B. S. 2011. An estimate of 1.9 Ga mantle depletion using the high-field-strength elements and Nd–Pb isotopes of ocean floor basalts, Flin Flon Belt, Canada. *Precambrian Research*, 189(1-2), 114-139. https://doi.org/10.1016/j.precamres.2011.05.006
4. Baublys, K. A., Golding, S. D., Young, E., & Kamber, B. S. 2004. Simultaneous determination of $\delta^{33}S_{V\text{-}CDT}$ and $\delta^{34}S_{V\text{-}CDT}$ using masses 48, 49 and 50 on a continuous flow isotope ratio mass spectrometer. *Rapid Communications in Mass Spectrometry*, 18(22), 2765-2769. https://doi.org/10.1002/rcm.1681
5. Brand, U., Posenato, R., Came, R., Affek, H., Angiolini, L., Azmy, K., & Farabegoli, E. 2012. The end-Permian mass extinction: A rapid volcanic CO_2 and CH_4-climatic catastrophe. *Chemical Geology*, 322, 121-144. https://doi.org/10.1016/j.chemgeo.2012.06.015
6. Cai, C., Worden, R. H., Bottrell, S. H., Wang, L., & Yang, C. 2003. Thermochemical sulphate reduction and the generation of hydrogen sulphide and thiols (mercaptans) in Triassic carbonate reservoirs from the Sichuan Basin, China. *Chemical Geology*, 202(1-2), 39-57. https://doi.org/10.1016/S0009-2541(03)00209-2
7. Carter, A., Roques, D., Bristow, C., & Kinny, P. 2001. Understanding Mesozoic accretion in Southeast Asia: significance of Triassic thermotectonism (Indosinian orogeny) in Vietnam. *Geology*, 29(3), 211-214. https://doi.org/10.1130/0091-7613(2001)029<0211:UMAISA>2.0.CO;2
8. Chen, J., & Chu, X. 1988. Sulfur isotope composition of Triassic marine sulfates of South China. *Chemical Geology: Isotope Geoscience section*, 72(2), 155-161. https://doi.org/10.1016/0168-9622(88)90063-2
9. Chen, Z. Q., & Benton, M. J. 2012. The timing and pattern of biotic recovery following the end-Permian mass extinction. *Nature Geoscience*, 5(6), 375-383. https://doi.org/10.1038/ngeo1475
10. Claypool, G. E., Holser, W. T., Kaplan, I. R., Sakai, H., & Zak, I. 1980. The age curves of sulfur and oxygen isotopes in marine sulfate and their mutual interpretation. *Chemical Geology*, 28, 199-260. https://doi.org/10.1016/0009-2541(80)90047-9
11. Courtillot, V., Jaeger, J. J., Yang, Z., Feraud, G. & Hofmann, C. 1996. The influence of continental flood basalts on mass extinctions: where do we stand?. *Geological Society of America Special Papers*, 307, 513-525. https://doi.org/10.1130/0-8137-2307-8.513
12. Eldholm, O., & Thomas, E. 1993. Environmental impact of volcanic margin formation. *Earth and Planetary Science Letters*, 117, 219-329. https://doi.org/10.1016/0012-821X(93)90087-P
13. Elrick, M., Polyak, V., Algeo, T. J., Romaniello, S., Asmerom, Y., Herrmann, A. D., Anbar, A. D., Zhao, L., & Chen, Z. Q. 2017. Global-ocean redox variation during the middle-late Permian through Early Triassic based on uranium isotope and Th/U trends of marine carbonates. *Geology*, 45(2), 163-166. https://doi.org/10.1130/G38585.1

14. Frogner, P., Gíslason, S. R., & Óskarsson, N. 2001. Fertilizing potential of volcanic ash in ocean surface water. *Geology*, 29(6), 487-490. https://doi.org/10.1130/0091-7613(2001)<0487:FPOVAI>2.0.CO;2
15. Gao, Q., Zhang, N., Xia, W., Feng, Q., Chen, Z. Q., Zheng, J., Griffin, W. L., O'Reilly, S. Y., Pearson, N. J., Wang, G., & Wu, S. 2013. Origin of volcanic ash beds across the Permian–Triassic boundary, Daxiakou, South China: petrology and U–Pb age, trace elements and Hf-isotope composition of zircon. *Chemical Geology*, 360, 41-53. https://doi.org/10.1016/j.chemgeo.2013.09.020
16. Gill, B. C., Lyons, T. W. & Saltzman, M. R. 2007. Parallel, high-resolution carbon and sulfur isotope records of the evolving Paleozoic marine sulfur reservoir. *Palaeogeography, Palaeoclimatology, Palaeoecology*, 256(3-4), 156-173. https://doi.org/10.1016/j.palaeo.2007.02.030
17. Gorjan, P., Kaiho, K., Kakegawa, T., Niitsuma, S., Chen, Z. Q., Kajiwara, Y., & Nicora, A. 2007. Paleoredox, biotic and sulfur-isotopic changes associated with the end-Permian mass extinction in the western Tethys. *Chemical Geology*, 244(3-4), 483-492. https://doi.org/10.1016/j.chemgeo.2007.07.003
18. Grard, A., Francois, L. M., Dessert, C., Dupré, B., & Godderis, Y. 2005. Basaltic volcanism and mass extinction at the Permo-Triassic boundary: environmental impact and modeling of the global carbon cycle. *Earth and Planetary Science Letters*, 234(1-2), 207-221. https://doi.org/10.1016/j.epsl.2005.02.027
19. Hallam, A. 1991. Why was there a delayed radiation after the end-Palaeozoic extinctions? *Historical Biology*, 5(2-4), 257-262. https://doi.org/10.1080/10292389109380405
20. Hu, S. X., Zhang, Q. Y., Chen, Z. Q., Zhou, C. Y., Lü, T., Xie, T., Wen, W., Huang, J. Y., & Benton, M. J. 2011. The Luoping biota: exceptional preservation, and new evidence on the Triassic recovery from end-Permian mass extinction. *Proceedings of the Royal Society B: Biological Sciences*, 278(1716), 2274-2282. https://doi.org/10.1098/rspb.2010.2235
21. Huang, K., Huang, S., Hu, Z., Zhong, Y., & Li, X. 2016. Carbon isotopic composition and evolution of the Lower Triassic marine carbonates from Dukou of Xuanhan and Beibei of Chongqing, Sichuan basin. *Journal of Palaeogeography*, 18(1), 101-114 (in Chinese with English abstract). doi: 10.7605/gdlxb.2016.01.008
22. Kaiho, K., Kajiwara, Y., Nakano, T., Miura, Y., Kawahata, H., Tazaki, K., Ueshima, M., Chen, Z., & Shi, G. R. 2001. End-permian catastrophe by a bolide impact: evidence of a gigantic release of sulfur from the mantle. *Geology*, 29(9), 815-818. https://doi.org/10.1130/0091-7613(2001)029<0815:EPCBAB>2.0.CO;2

23. Kamo, S. L., Czamanske, G. K., Amelin, Y., Fedorenko, V. A., Davis, D. W., & Trofimov, V. R. 2003. Rapid eruption of Siberian flood-volcanic rocks and evidence for coincidence with the Permian–Triassic boundary and mass extinction at 251 Ma. *Earth and Planetary Science Letters*, 214(1-2), 75-91. https://doi.org/10.1016/S0012-821X(03)00347-9
24. Kampschulte, A., & Strauss, H. 2004. The sulfur isotopic evolution of Phanerozoic seawater based on the analysis of structurally substituted sulfate in carbonates. *Chemical Geology*, 204(3-4), 255-286. https://doi.org/10.1016/j.chemgeo.2003.11.013
25. Klinkhammer, G. P., & Palmer, M. R. 1991. Uranium in the ocean: Where it goes and why? *Geochimica et Cosmochimica Acta*, 7, 1799-1806. https://doi.org/10.1016/0016-7037(91)90024-Y
26. Knoll, A. H., Bambach, R. K., Canfield, D. E., & Grotzinger, J. P. 1996. Comparative Earth history and Late Permian mass extinction. *Science*, 273(5274), 452-457. doi: 10.1126/science.273.5274.452
27. Kockum, P. C. F., Herbert, R. B., & Gislason, S. R. 2006. A diverse ecosystem response to volcanic aerosols. *Chemical Geology*, 231(1-2), 57-66. https://doi.org/10.1016/j.chemgeo.2005.12.008
28. Kramm, U., & Wedepohl, K. H. 1991. The isotopic composition of strontium and sulfur in seawater of Late Permian (Zechstein) age. *Chemical Geology*, 90(3-4), 253-262. https://doi.org/10.1016/0009-2541(91)90103-X
29. Kump, L. R., Pavlov, A., & Arthur, M. A. 2005. Massive release of hydrogen sulfide to the surface ocean and atmosphere during intervals of oceanic anoxia. *Geology*, 33(5), 397-400. https://doi.org/10.1130/G21295.1
30. Li, L., Tan, X., Cao, J., Zou, C., Ding, X., Yang, G., & Ying, D. 2014. Origins of evaporites in the Middle Triassic Leikoupo Formation of the Sichuan Basin, southwest China and their geological implications. *Carbonates and Evaporites*, 29(1), 55-63. https://doi.org/10.1007/s13146-013-0169-y
31. Lo, C. H., Chung, S. L., Lee, T. Y., & Wu, G. 2002. Age of the Emeishan flood magmatism and relations to Permian–Triassic boundary events. *Earth and Planetary Science Letters*, 198(3-4), 449-458. https://doi.org/10.1016/S0012-821X(02)00535-6
32. Looy, C. V., Brugman, W. A., Dilcher, D. L., & Visscher, H. 1999. The delayed resurgence of equatorial forests after the Permian–Triassic ecologic crisis. *Proceedings of the national Academy of Sciences*, 96(24), 13857-13862. https://doi.org/10.1073/pnas.96.24.13857
33. Maruoka, T., Koeberl, C., Hancox, P. J., & Reimold, W. U. 2003. Sulfur geochemistry across a terrestrial Permian–Triassic boundary section in the Karoo Basin, South Africa. *Earth and Planetary Science Letters*, 206(1-2), 101-117. https://doi.org/10.1016/S0012-821X(02)01087-7
34. Meng, Q. R., & Zhang, G. W. 1999. Timing of collision of the North and South China blocks: controversy and reconciliation. *Geology*, 27(2), 123-126. https://doi.org/10.1130/0091-7613(1999)027<0123:TOCOTN>2.3.CO;2

35. McArthur, J. M., Howarth, R. J., & Bailey, T. R. 2001. Strontium isotope stratigraphy: LOWESS version 3: best fit to the marine Sr-isotope curve for 0–509 Ma and accompanying look-up table for deriving numerical age. *The Journal of Geology*, 109(2), 155-170. https://doi.org/10.1086/319243
36. McArthur, J. M., Howarth, R. J., & Shields, G. A. 2012. Strontium isotope stratigraphy. In: Gradstein F. M., Ogg, J. G., Schmitz, M. D., Ogg, G. M., eds., *The geologic time scale*. 127-144. https://doi.org/10.1017/CBO9780511536045.008
37. Newton, R. J., Pevitt, E. L., Wignall, P. B., & Bottrell, S. H. 2004. Large shifts in the isotopic composition of seawater sulphate across the Permo–Triassic boundary in northern Italy. *Earth and Planetary Science Letters*, 218(3-4), 331-345. https://doi.org/10.1016/S0012-821X(03)00676-9
38. Niu, Y., & Batiza, R. 1997. Trace element evidence from seamounts for recycled oceanic crust in the Eastern Pacific mantle. *Earth and Planetary Science Letters*, 148(3-4), 471-483. https://doi.org/10.1016/S0012-821X(97)00048-4
39. Olsen, P. E. 1999. Giant lava flows, mass extinctions, and mantle plumes. *Science*, 284(5414), 604-605. doi: 10.1126/science.284.5414.604
40. Payne, J. L., Lehrmann, D. J., Wei, J., Orchard, M. J., Schrag, D. P., & Knoll, A. H. 2004. Large perturbations of the carbon cycle during recovery from the end-Permian extinction. *Science*, 305(5683), 506-509. doi: 10.1126/science.1097023
41. Payne, J. L., & Kump, L. R. 2007. Evidence for recurrent Early Triassic massive volcanism from quantitative interpretation of carbon isotope fluctuations. *Earth and Planetary Science Letters*, 256(1-2), 264-277. https://doi.org/10.1016/j.epsl.2007.01.034
42. Present, T. M., Paris, G., Burke, A., Fischer, W. W., & Adkins, J. F. 2015. Large carbonate associated sulfate isotopic variability between brachiopods, micrite, and other sedimentary components in Late Ordovician strata. *Earth and Planetary Science Letters*, 432, 187-198. https://doi.org/10.1016/j.epsl.2015.10.005
43. Renne, P. R., & Basu, A. R. 1991. Rapid eruption of the Siberian Traps flood basalts at the Permo-Triassic boundary. *Science*. 253(5016), 176-179. Doi: 10.1126/science.253.5016.176
44. Renne, P. R., Black, M. T., Zichao, Z., Richards, M. A., & Basu, A. R. 1995. Synchrony and causal relations between Permian-Triassic boundary crises and Siberian flood volcanism. *Science*, 269(5229), 1413-1416. Doi: 10.1126/science.269.5229.1413
45. Riccardi, A. L., Arthur, M. A., & Kump, L. R. 2006. Sulfur isotopic evidence for chemocline upward excursions during the end-Permian mass extinction. *Geochimica et Cosmochimica Acta*, 70(23), 5740-5752. https://doi.org/10.1016/j.gca.2006.08.005

46. Richter, F. M., Rowley, D. B., & DePaolo, D. J. 1992. Sr isotope evolution of seawater: the role of tectonics. *Earth and Planetary Science Letters*, 109(1-2), 11-23. https://doi.org/10.1016/0012-821X(92)90070-C
47. Scotese, C. R., & Golonka, J. 1997. Paleogeographic atlas. PALEOMAP Project, University of Texas at Arlington, 1-45.
48. Shen, S. Z., Crowley, J. L., Wang, Y., Bowring, S. A., Erwin, D. H., Sadler, P. M., Cao, C. Q., Rothman, D. H., Henderson, C. M., Ramezani, J., & Zhang, H. 2011. Calibrating the end-Permian mass extinction. *science*, 334(6061), 1367-1372. Doi: 10.1126/science.1213454
49. Sim, M. S., Ono, S., & Hurtgen, M. T. 2015. Sulfur isotope evidence for low and fluctuating sulfate levels in the Late Devonian ocean and the potential link with the mass extinction event. *Earth and Planetary Science Letters*, 419, 52-62. https://doi.org/10.1016/j.epsl.2015.03.009
50. Song, H., Tong, J., Algeo, T. J., Song, H., Qiu, H., Zhu, Y., Tian, L., Bates, S., Lyons, T. W., Luo, G., & Kump, L. R. 2014. Early Triassic seawater sulfate drawdown. *Geochimica et Cosmochimica Acta*, 128, 95-113. https://doi.org/10.1016/j.gca.2013.12.009
51. Song, H., Wignall, P. B., Tong, J., Song, H., Chen, J., Chu, D., Tian, L., Luo, M., Zong, K., Chen, Y., & Lai, X. 2015. Integrated Sr isotope variations and global environmental changes through the Late Permian to early Late Triassic. *Earth and Planetary Science Letters*, 424, 140-147. https://doi.org/10.1016/j.epsl.2015.05.035
52. Strauss, H. 1999. Geological evolution from isotope proxy signals—sulfur. *Chemical Geology*, 161(1-3), 89-101. https://doi.org/10.1016/S0009-2541(99)00082-0
53. Sun, Y., Gao, Y., Wang, D., Dai, H., Gu, W., Li, J., & Zhang, L. 2017. Zircon U-Pb dating of "Mung Bean Rock" in the Tongliang Area, Chongqing and Its geological significance. *Rock and Mineral Analysis*, 36(6), 649-658 (in Chinese with English abstract). doi: 10.15898/j.cnki.11-2131/td.201702220022
54. Sun, Y., Joachimski, M. M., Wignall, P. B., Yan, C., Chen, Y., Jiang, H., Wang, L., & Lai, X. 2012. Lethally hot temperatures during the Early Triassic greenhouse. *Science*, 338(6105), 366-370. Doi: 10.1126
55. Tan, X., Li, L., Liu, H., Cao, J., Wu, X., Zhou, S., & Shi, X. 2014. Mega-shoaling in carbonate platform of the Middle Triassic Leikoupo Formation, Sichuan Basin, Southwest China. *Science China, Earth Science*, 57(3), 465-479. https://doi.org/10.1007/s11430-013-4667-5
56. Tostevin, R., Turchyn, A. V., Farquhar, J., Johnston, D. T., Eldridge, D. L., Bishop, J. K. & McIlvin, M. 2014. Multiple sulfur isotope constraints on the modern sulfur cycle. *Earth and planetary science letters*, 396, 14-21. https://doi.org/10.1016/j.epsl.2014.03.057

57. Veizer, J., Buhl, D., Diener, A., Ebneth, S., Podlaha, O. G., Bruckschen, P., Jasper, T., Korte, C., Schaaf, M., & Ala, D., Azmy, K. 1997. Strontium isotope stratigraphy: potential resolution and event correlation. *Palaeogeography, Palaeoclimatology, Palaeoecology*, 132(1-4), 65-77. https://doi.org/10.1016/S0031-0182(97)00054-0

58. Visscher, H., Looy, C. V., Collinson, M. E., Brinkhuis, H., van Konijnenburg-van Cittert, J. H. A., Kürschner, W. M., & Sephton, M. A. 2004. Environmental mutagenesis during the end-Permian ecological crisis. *Proceedings of the National Academy of Sciences*, 101(35), 12952-12956. https://doi.org/10.1073/pnas.0404472101

59. Weyer, S., Anbar, A. D., Gerdes, A., Gordon, G. W., Algeo, T. J., & Boyle, E. A. 2008. Natural fractionation of $^{238}U/^{235}U$. *Geochimica et Cosmochimica Acta*, 72, 345-359. https://doi.org/10.1016/j.gca.2007.11.012

60. Wotte, T., Shields-Zhou, G. A., & Strauss, H. 2012. Carbonate-associated sulfate: experimental comparisons of common extraction methods and recommendations toward a standard analytical protocol. *Chemical Geology*, 326, 132-144. https://doi.org/10.1016/j.chemgeo.2012.07.020

61. Zhu, J. 1990. The features and their significance of carbon and oxygen isotopes in the saline formation of Triassic, Huaying Mountain, Sichuan Province. *Acta Petrologica Sinica*, 4, 67-71 (in Chinese with English abstract).

62. Zhu, Z., & Wang, G. 1986. Paleogeography of before and after deposition of green-bean rock (altered tuff) between the Early and Middle Triassic in the Upper Yangtze Platform and its adjacent areas. *Oil & Gas Geology*, 7(4): 344-355 (in Chinese with English abstract).